Journal of Engineering and Technology for Industrial Applications

ISSN ONLINE: 2447-0228

ITEGAM-JETIA

Manaus, v.12 n.57, p.705-717. January/February, 2026.
DOI: https://doi.org/10.5935/jetia. v12i57.3032

RESEARCH ARTICLE OPEN ACCESS

DC-BUS CAPACITOR DISCHARGE CONTROL STRATEGY FOR PMSM DRIVES SYSTEM: ELECTRIC VEHICLES

Chevuru Mahima*[1], Ch. Chengaiah[2]

[1]Department of Power Systems Engineering, India.
[2]Sri Venkateswara University College of Engineering, S V University, Tirupati, India. 517502.

[1]https://orcid.org/0009-0003-0929-7074, [2]https://orcid.org/0000-0002-4604-9497

Email: *chevurumahima@gmail.com, chinthapudisvu@gmail.com

ARTICLE INFO

Article History
Received: December 1, 2025
Revised: January 10, 2026
Accepted: January 15, 2026
Published: February 28, 2026

Keywords:
Permanent Magnet Synchronous Machine (PMSM),
DC- bus discharge,
Extended state observer (ESO), ANN,
Adaptive Neuro-Fuzzy Inference System (ANFIS) etc.

ABSTRACT

Electric vehicles have become increasingly popular for their high efficiency and zero emissions, making them vital for sustainable transportation. The Permanent Magnet Synchronous Motors (PMSM) are widely used in Electric Vehicles, because of the Active discharge mechanism play a critical role in maintaining the safety and reliability of Electric Vehicle (EV) system. The proposed control strategy ensures that, the DC bus capacitor voltage is safely discharged to an acceptable level during emergency fault conditions. This paper proposed a robust winding-based capacitor discharge strategy that effectively utilizes the inherent machine windings of the PMSM as an alternative discharge path when the active circuit is unavailable. The control strategy discharge mechanism operates in two distinct stages to ensure rapid and controlled voltage reduction. In the first stage, a large flux-enfeebling in d-axis current which is injected to quickly suppress the back electromotive force (EMF), thereby achieving an immediate reduction in the DC bus voltage. In the second stage, a voltage regulation process compensates for residual energy caused by switching losses and inductive effects, maintaining the voltage at a safe level until the system stabilizes. This approach eliminates the dependence on external resistors for improving the system safety and cost-effectiveness. During normal operation to enhance the dynamic performance of the electric vehicle system, a PMSM drive systems with an integrated ANFIS controller is used for speed regulation. The proposed control strategy synergizes the adaptive learning capability of neural networks with the rule-based reasoning of fuzzy logic, to resulting in improved nonlinear control characteristics compared with PI, FUZZY and ANN Controllers. This paper presents the design and simulation of an PMSM drive system with ANFIS based speed control for EV system. To validate the effectiveness of the proposed system, the MATLAB Simulink model is implemented on a three-phase Surface-mounted PMSM (SPMSM) drive platform. The PMSM drive with ANFIS-controller, exhibits precise and stable speed control, even under rapid transients and varying load conditions and enhanced performance during standard operation offering a reliable, intelligent and cost-efficient solution for modern electric vehicle drive systems.

I. INTRODUCTION

The permanent magnet synchronous motor (PMSM) is commonly used as the power train in electric vehicles [1-4] due to on hand benefits, such as high efficiency, high torque density, and excellent torque ratios [5-9]. Additionally to enhance the driving efficiency of PMSMs and minimize the driving currents increasingly rely on high-voltage drive systems [10]. However, high-voltage power train pose a risk of electric shock to the driver in the event of an emergency, such as a car crash, to address this concern, the United Nations Vehicle Regulation ECC R94 mandates that the DC bus capacitor voltage is reduced to safe level with a short duration [11], [12].

The winding-based discharge method can not only reduce the volume of the discharge circuit but also be cost- effective [13-15]. The schematic block diagram of the EV powertrain actuation system as shown in Figure 1. The topology of an Electric Vehicle (EV) powertrain employing a Permanent Magnet Synchronous Motor (PMSM). The system includes a battery pack, DC–DC boost converter, inverter, PMSM, and gearbox. The battery supplies DC power, which is boosted and converted into three-phase AC by the inverter to drive the PMSM. The motor output is transmitted to the wheels through the gearbox.

A breaker is incorporated for safety and is tripped during emergencies or crashes to isolate the battery, ensuring system protection and operational safety. A dc-bus voltage regulator based on a proportional integral controller and a modulation index controller are used to generate the reference d-axis current in order to stop the bus voltage. A fixed d-axis current and piecewise q-axis current control is suggested in [16] with the goal of discharging the capacitor voltage of specific EV driven systems with large inertia and minimal safe current. Furthermore, the synchronous reference frame of the three-phase PWM rectifier model is nonlinear, making the ANFIS based approach inapplicable to the system. The purpose of this study is to provide a reliable dc-bus capacitor discharge method for PMSM EV drives in the event of a discharge circuit failure. To achieve the dc-bus voltage constant and prevent voltage spikes, the measured total disturbance is instantly corrected to the dc-bus capacitor energy loop control law.

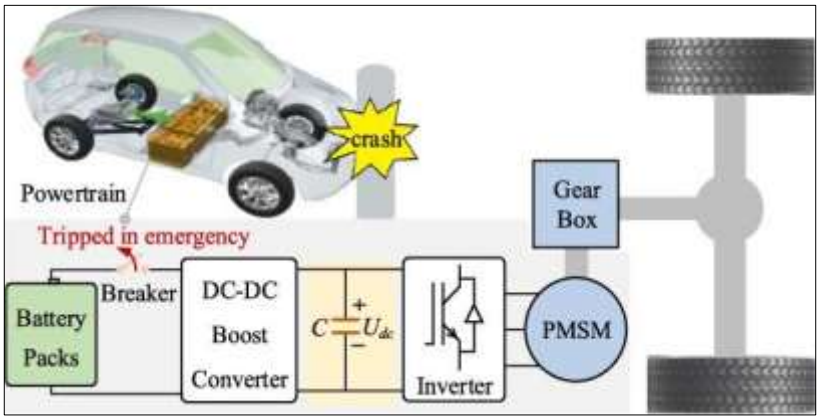

Figure1: Schematic diagram of PMSM-EV powertrain systems.
Source: Authors, (2026).

In the event of an emergency involving electric vehicles, a malfunctioning or failed bleeding resistor can pose serious risks of electric shock to both passengers and rescuers. To enhance EV safety, a practical solution is to implement advanced discharge circuit fault-handling techniques. These techniques ensure that the discharge process adheres to critical safety standards, such as completing discharge within five seconds while preventing voltage surges. By integrating these safeguards, the risk of high-voltage exposure can be significantly minimized, making emergency responses safer and more effective. To stabilize the voltage, ESO is used to monitor the dc-bus capacitor energy until the voltage drops to zero. The active disturbance rejection observer, which includes ESO [17]. The mathematical model of the Permanent Magnet Synchronous Motor (PMSM) in the rotating dq-reference frame is employed because it accurately represents both the electrical and mechanical dynamics of the motor during the capacitor discharge operation. The following equations describe the stator voltage, current variation, and torque production in the PMSM [18-20].

$$\begin{cases} u_d = R_s i_d + L_s \dfrac{di_d}{dt} - \omega_e L_s i_q \\ u_q = R_s i_q + L_s \dfrac{di_q}{dt} + \omega_e L_s i_d + \omega_e \psi_f \\ T_e = \dfrac{3}{2} p \psi_f i_q \end{cases} \tag{1}$$

Where i_d, i_q and u_d, u_q: d axis and q-axis of stator currents and voltages, L_s: stator inductance, R_s: Stator resistance, ω_e: electrical angular velocity, p: pole pair, ψ_f: flux linkage T_e: electromagnetic torque. Under steady state condition the mechanical equation of the permanent magnet synchronous motor can be expressed as,

$$J \frac{d\omega_m}{dt} = T_e - B_m \omega_m \tag{2}$$

Where ω_m : mechanical angular velocity, J and B_m: inertia and mechanical damping coefficient. Under dynamic state condition the dc capacitor voltage u_{dc} can be expressed based on the 3-phase inverter circuit which is shown in Figure 2

$$C \frac{du_{dc}}{dt} = i_{dc} \tag{3}$$

Where i_{dc} and u_{dc} stand for the dc-bus current and voltage, respectively, and C is the capacitor.

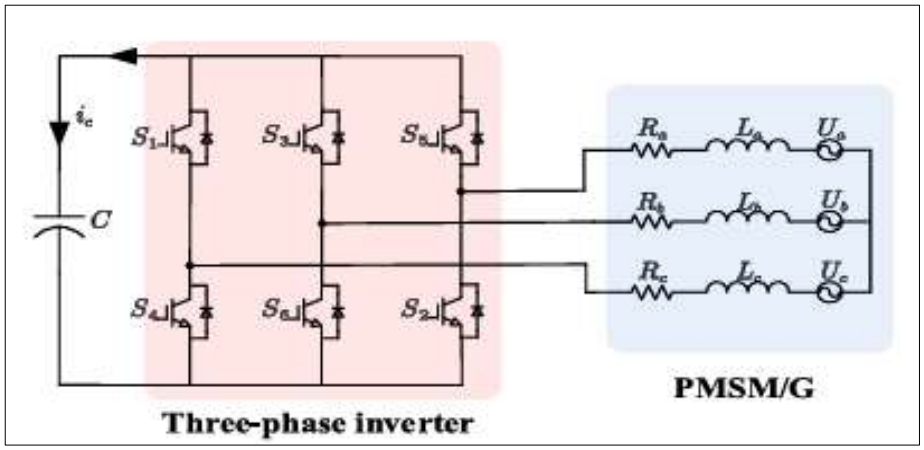

Figure 2: Three phase inverter with PMSM winding based dc-bus capacitor.
Source: Authors, (2026).

The Figure 2 shows that the three phase inverter with PMSM winding based dc bus capacitor discharge, however from the basic fundamentals the converter's power loss, the AC side's power should match the DC side's power, which means

$$u_{dc}i_{dc} + P_{con} = -\frac{3}{2}\left(u_d i_d + u_q i_q\right) \tag{4}$$

Where p_{con}: Power switching loss. To examine the power flow process during discharge, substitute (1) and (3) equations into the instantaneous power balance equation (4).

$$\frac{d}{dt}\left(\frac{1}{2}Cu_{dc}^2\right) = -\frac{3}{2}\omega_e\psi_f i_q - \frac{3}{2}R_s\left(i_d^2 + i_q^2\right) - \frac{3}{2}\left(L_s i_q\frac{di_q}{dt} + L_s i_d\frac{di_d}{dt}\right) - P_{con} \tag{5}$$

From equation. (5) it is observed that, a portion of the permanent magnet synchronous motor's electromagnetic power output is converted to inductance coil energy, copper winding loss, and converter loss. The capacitor's energy storage is then modified using the residual.

II. PROPOSED MODEL OF THE ROBUST WINDING BASED DISCHARGE METHOD

When EVs experience an emergency with an active discharge circuit defect, it's critical to redesign a robust discharge strategy in order to achieve a safe and dependable discharge technique. Thus, this section presents a reliable winding-based dc-bus capacitor discharge method based on ESO.

II.1 RAPID DISCHARGE STATE:

When an active discharge is needed, it is significant and safe for both passengers and rescuers if the dc-bus voltage can drop to safe levels right away. When an emergency occurs in an electric car, the back electromotive force (EMF) is more than the safe voltage because the motor speed is higher. Due to the dc-bus capacitor voltage follow the back EMF, the dc-bus capacitor voltage can drop to safe voltage when the back EMF is reduced to safe voltage. According to the flux-enfeebling principle, a large d-axis current is injected to rapidly reduce the EMF because the dc-bus voltage is proportional to the PMSM's EMF. At the same time, the q-axis current remains at zero to stop the conversion of kinetic energy into electrical energy [21]. From EVs PMSM powertrain system which is shown in fig.1. The dc-bus voltage is expressed as

$$u_{dc} = \sqrt{3}\omega_e\left(\psi_f + L_s i_d\right) - R_s\sqrt{i_d^2 + i_q^2} - 2V_{on} \tag{6}$$

Where V_{on} : diode conducted voltage. The voltage should decrease to a safe level during the rapid discharge stage. Then, the flux-enfeebling current on the d-axis is expresse

$$i_d^* = \frac{U_{safe} - \sqrt{3}\omega_e\psi_f}{\left(\sqrt{3}\omega_e L_s + R_s\right)} \tag{7}$$

Where U_{safe} : safe voltage 60V. Consequently, once the active discharge is needed, the estimated d-axis current can be injected to lower the dc-bus voltage to the safe voltage. A zero q-axis current is applied concurrently to stop any electromagnetic power from turning into electrical energy.

II.2 BUS VOLTAGE CONTROL STAGE ON ESO

The Extended State Observer (ESO) is a powerful control method widely used to manage disturbances and enhance the robustness of dynamic systems, particularly in challenging environments in electric vehicle (EV) powertrains. In the context of Permanent Magnet Synchronous Motor (PMSM) drives, the ESO plays a crucial role in managing uncertainties, compensating for system disturbances, and improving control precision. When the DC-bus voltage reaches 60 V, the ESO-based voltage control stage is activated. To maintain the voltage within a safe range 60 V the controller regulates the discharge process and ensures stable operation, a robust voltage control loop is designed. Since the energy flow during the discharge mode described in Equation (5) exhibits nonlinear characteristics, the PI, FUZZY controller is unable to produce adequate results, particularly when motor parameters will alter during the discharging mode to overcome this ANFIS with ESO-based ultra-local model is introduced to effectively address this issue. For converting Equation (5) into an integral series form, the first-order ultra-local model of a single-input and single-output system is defined as given in [22–25].

$$y^{\cdot} = F + \alpha u \tag{8}$$

Where F Stands for known and unknown components of the system, u : control variables, y : output variables, and α : nonphysical scaling factor. This article's mathematical model of the energy flow-based ESO can be stated using formulas (5) and (8).

$$\frac{dE_c}{dt} = F + \alpha u \tag{9}$$

Where E_c: $0.5Cu^2_{dc}$, u: i_q, α: $-1.5\omega_e\psi_f$ and the other terms on the right side of equation (5) except $-1.5\omega_e\psi_f i_q$ are treated as the total disturbance and notated as F

$$F = -\frac{3}{2}R_s\left(i_d^2 + i_q^2\right) - \frac{3}{2}\left(L_s i_q \frac{di_q}{dt} + L_s i_d \frac{di_d}{dt}\right) - P_{con} \tag{10}$$

Equation (10), shows that the total disturbance corresponds to the overall power loss, which includes switching loss, winding copper loss, and inductive coil energy storage. It is assumed that *F* remains constant during each sampling period. A linear equation of ESO, can be formulated based on the ultra-local model, which is shown in fig.4 proportionately considering E_c and F as a variables given in Equation (8) is expressed as.

$$\begin{cases} e_1 = z_1 - E_c \\ \dot{z}_1 = z_2 - \beta_1 e_1 + \alpha u \\ \dot{z}_2 = -\beta_2 e_2 \end{cases} \tag{11}$$

Where z_1 and z_2: estimated value of E_c and F. β_1 and β_2: feedback gains it can be estimate the real-time value of E_c and F that is, $Z_1 \rightarrow E_C$; $Z_2 \rightarrow F$. From the above mathematical model analysis the winding based DC- bus capacitor discharge is implemented with proposed control strategy mechanism is described with ANFIS and ESO which is described in the subsequent sections.

III. WINDING BASED DC BUS CAPACITOR DISCHARGE STRATEGY WITH ANFIS

The conventional and suggested discharge methods using the dc-bus voltage controller based on ESO. It also presents the suggested resilient dc- bus capacitor discharge strategy. The proposed winding based dc-bus capacitor discharge control system as shown in fig.3 and the corresponding bus voltage control strategy on ESO of internal diagram as shown in fig.4. The proposed strategy consists of two stages. In the rapid discharge stage, a large flux-enfeebling d-axis current is injected into the motor, reducing the back electromotive force (EMF) and consequently lowering the dc-bus voltage to a predefined safe threshold. During this stage, the q-axis current is maintained at zero to prevent additional energy conversion from mechanical to electrical form.

Once the safe voltage is reached, the process transitions into the voltage regulation stage. During normal driving, Port-1 is turned ON the motor uses vector control to run the vehicle, while the ESO helps the current follow the reference smoothly. When the system receives a discharge command, Port-2 is turned ON, and the ESO-based discharge control is used to safely and quickly reduce the dc-bus capacitor voltage through the motor windings [26]. ANFIS are used in the d-axis and q-axis current loops so that the current can respond fast and accurately in both normal operation and discharge mode. Where as ESO is employed to estimate and compensate for system disturbances such as copper losses, switching losses and inductive energy storage

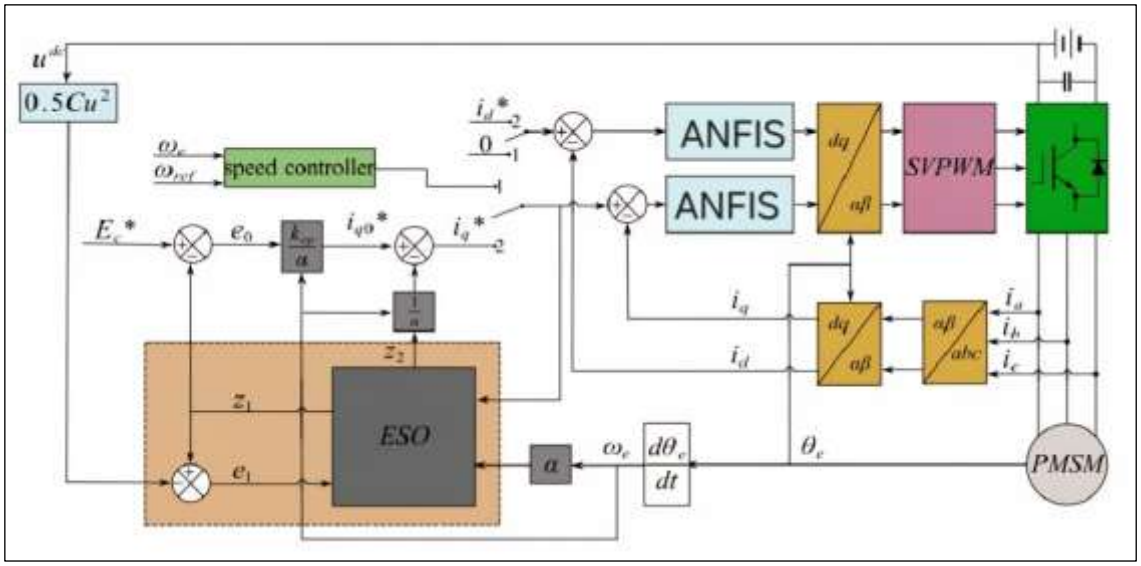

Figure 3: Block diagram of the winding based dc bus capacitor discharge strategy.
Source: Authors, (2026).

The ESO shown in the above block diagram fig.3 is represented as a subsystem in the fig.4 below, showing its internal structure.

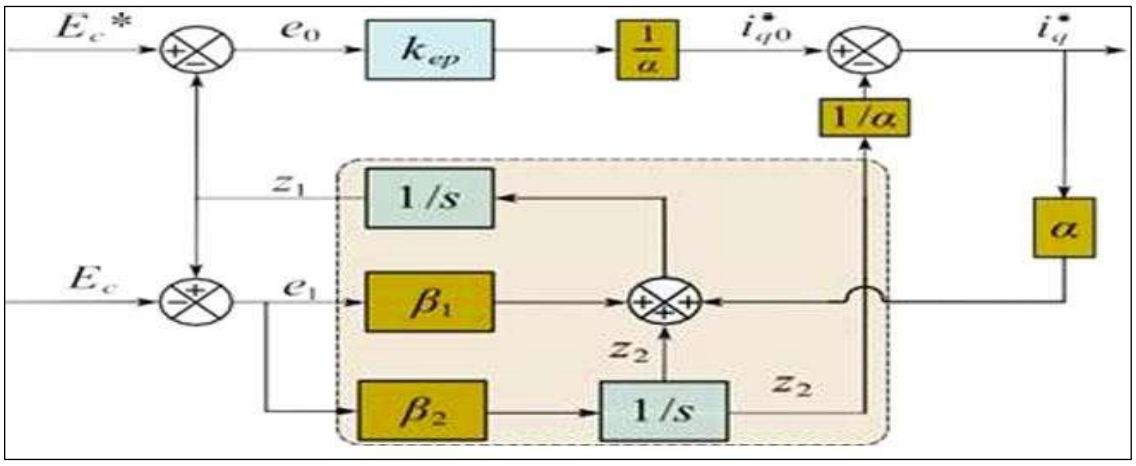

Figure 4: Bus voltage control strategy on Extended State Observer (ESO).
Source: Authors, (2026).

The ESO-based design enhances the robustness of the discharge control by effectively addressing nonlinear dynamics and parameter variations that conventional PI controllers cannot handle. In addition to ensuring safety under emergency conditions, maintaining high performance under normal operating modes is equally important for EV traction systems [27]. This work also incorporates an Adaptive Neuro-Fuzzy Inference System (ANFIS) controller for PMSM speed regulation. The ANFIS controller combines the self-learning capability of neural networks with the reasoning ability of fuzzy logic. This hybrid intelligent control strategy improves dynamic response, robustness, and overall stability of the PMSM drive during normal operation.

IV. PROPOSED ADAPTIVE NEURO FUZZY INFERENCE SYSTEM (ANFIS) CONTROLLER

Fig.5 shows that an Adaptive Neuro-Fuzzy Inference System (ANFIS) consists of a five-layer feed-forward structure that integrates the human-interpretable fuzzy logic framework with the adaptive learning capability of neural networks. Each layer performs a specific computational function in the Sugeno-type fuzzy inference process. The rules are expressed which is shown in table.1

Table:1 Sugeno ANFIS Rule Base.

Rule	Antecedent (IF …)	Consequent (THEN …)
R1	If (x) is (A_1)	($f_1 = p_1x + q_1$)
R2	If (x) is (A_2)	($f_2 = p_2x + q_2$)
R3	If (x) is (A_3)	($f_3 = p_3x + q_3$)

Source: Authors, (2026).

Here, $\boldsymbol{A_1}, \boldsymbol{A_2}$,and $\boldsymbol{A_3}$ denote the three membership functions corresponding to the input variable. The parameters $\boldsymbol{p_i}$ and $\boldsymbol{q_i}$ represent the consequent parameters, which are tuned during the learning process to achieve optimal system performance.

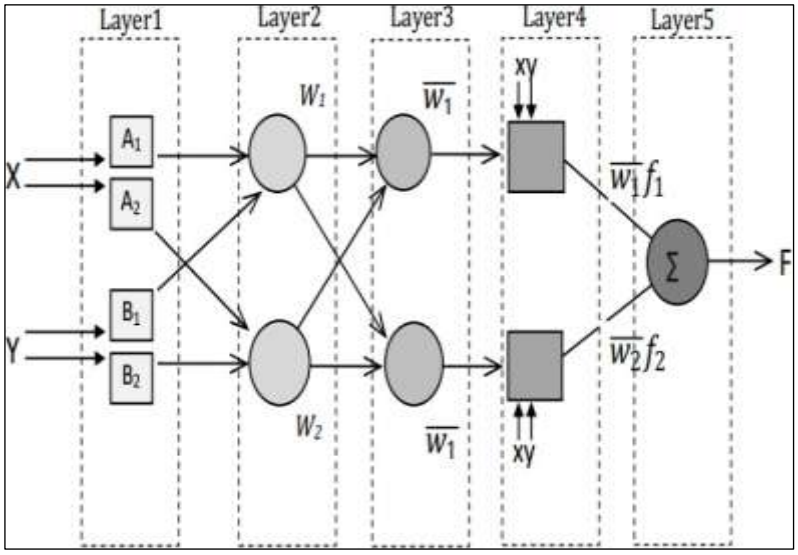

Figure 5: Rule based Adaptive Nuero Fuzzy Inference System.
Source: Authors, (2026).

From the fig.5 it is observe that the five-layer structure of a typical Sugeno-type ANFIS model.

Layer 1: Fuzzification Layer (Input Membership Functions)

This layer transforms the crisp input variables into fuzzy values by evaluating their membership degrees. Each neuron corresponds to a linguistic term such as Negative, Zero, or Positive. The output of this layer is:

$$O_{1,i} = \mu_{A_i}(x) \tag{12}$$

Where $\mu_{A_i}(x)$denotes the membership grade of input $x$to fuzzy set A_i. The parameters of this layer are called premise parameters, which are tuned during training.

Layer 2: Rule Layer (Firing Strength Computation)

Each neuron in this layer represents a fuzzy rule. The nodes multiply the incoming fuzzified signals to compute the firing strength of each rule. For a 2-input system:

$$O_{2,i} = w_i = \mu_{A_i}(x) \cdot \mu_{B_i}(y) \tag{13}$$

Thus, this layer models fuzzy logic's AND operation using the product operator.

Layer 3: Normalization Layer

This layer normalizes the firing strengths of all rules to ensure they sum to one. The normalized weight for rule $i$is calculated as:

$$O_{3,i} = \bar{w}_i = \frac{w_i}{\sum_{k=1}^{n}.w_k} \tag{14}$$

This normalization reflects the contribution level of each rule in the inference process.

Layer 4: Consequent Layer (Sugeno Rule Output)

Each neuron in this layer generates the rule's output based on a first-order Sugeno fuzzy model. The output of this layer is:

$$O_{4,i} = \bar{w}_i f_i = \bar{w}_i(p_i x + q_i y + r_i) \tag{15}$$

Here, p_i, q_i, and r_i are consequent parameters, trained together with premise parameters using a hybrid learning algorithm.

Layer 5: Output Layer (Defuzzification)

This layer aggregates the weighted outputs of all rules to obtain a single crisp system output. The output is computed as:

$$O_5 = \sum_{i=1}^{n}.\bar{w}_i f_i \tag{16}$$

Thus, Layer 5 performs defuzzification through a weighted average, delivering the final ANFIS prediction or control action. From section I to section IV are integrated based on the scope of the proposed control strategy of PMSM with EV system is tested in MATLAB Simulink Environment which described elaborately in the subsequent section in this paper.

V. TESTING OF SIMULINK BLOCK WITH PROPOSED METHOD

The Simulink block implemented by integrating of PMSM dc bus capacitor winding based with ESO and ANFIS which is shown in the fig.6 and it demonstrates the dual benefits of the winding-based capacitor discharge method and the ANFIS speed regulation strategy for PMSM-driven electric vehicles. The parameters of the PMSM Simulink model as shown in table.2. The Simulink block consists of the main functional subsystems required for the proposed robust dc-bus capacitor discharge control. The power supply section includes the fuel cell and battery connected through a bidirectional DC/DC converter. The power inverter drives the Permanent Magnet Synchronous Machine (PMSM) using space-vector pulse-width modulation (SVPWM).

The motor control strategy is implemented using an ANFIS-based speed controller along with d-q axis current controllers for accurate torque and current tracking. An Extended State Observer (ESO) is integrated to estimate disturbances and maintain dc-bus voltage stability during discharge events. Additionally, an electric braking interface and sensor feedback loops are included to ensure safety and smooth operational transitions between normal driving and discharge mode. From stable operation the EV battery fuel systems charging with an SOC condition. Once discharge the system automatically switches back to normal operation, where the fuel cell supplies power to the dc-bus and recharges the battery. This ensures a smooth transition and efficient recovery of the vehicle's energy.

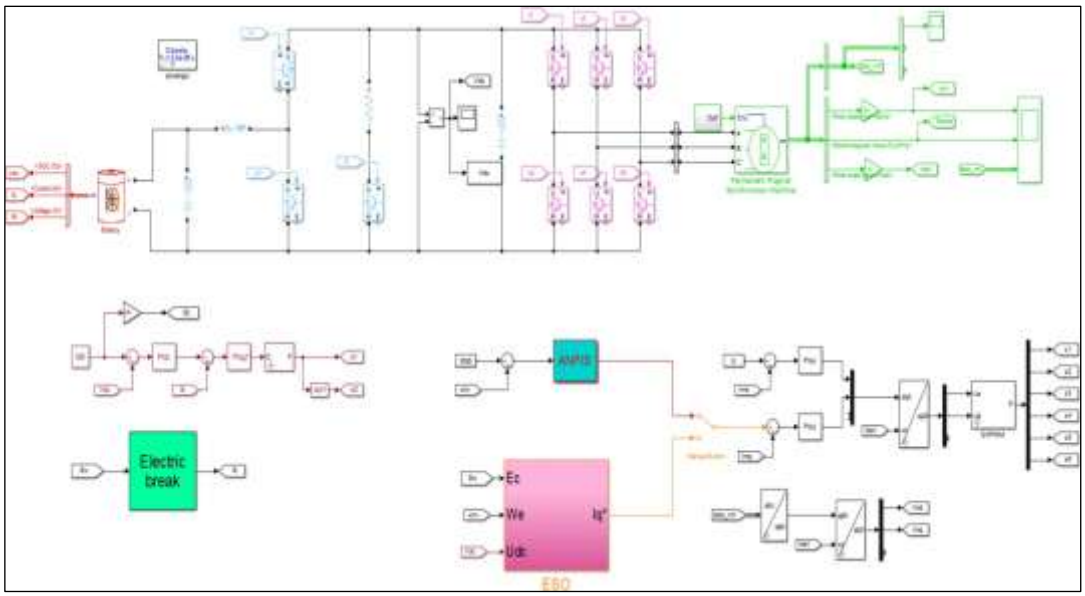

Figure 6: Simulation designing of proposed PMSM drive using ANFIS for EV.
Source: Authors, (2026).

Table:2 Parameters of PMSM.

Parameter	Symbol	Value
DC Bus Capacitor	C	$420\mu_F$
DC Bus Voltage	V_{dc}	320V
Stator Resistance	R_s	0.2 Ω
d-axis Inductance	L_d	1.5 mH
q-axis Inductance	L_q	2.0 mH
Permanent Magnet Flux	ψ_f	0.12 Wb
Pole Pairs	p	4
Rotor Inertia	J	0.01 kgm²
Load Torque	T_{load}	10 - 50 Nm
Motor speed	ω_m	1000rpm

Source: Authors, (2026).

During the emergency scenario, the capacitor discharge process was initiated by injecting a large flux- enfeebling current through the stator windings, where the Extended State Observer (ESO) played a vital role in estimating system uncertainties such as copper losses, switching effects, and residual inductive energy. By compensating for these disturbances, the ESO ensured that the dc-bus voltage was held within a safe operating margin, preventing any rebound or unsafe levels of stored energy. However the Simulink model is tested and the corresponding test results are analyzed based on the speed regulation, torque, stator voltage, stator current as a case study 1. Steady state operation and 2. Dynamic state operation.

Case:I The steady state behavior of the PMSM drive system: ANFIS with EV

In this case, the steady-state performance of the ANFIS-controlled PMSM drive is evaluated at 1000 rpm under constant load that is 25 Nm. The controller accurately maintained the reference speed with negligible error and ensured stable dc-bus voltage (320V), battery voltage (130V), and current (25A,). The dq-axis currents remained steady, providing effective flux and torque control, while the electromagnetic torque showed 25Nm output with minimal ripple. The corresponding test output results speed characteristics 7(a), torque characteristics 7(b), DC bus voltage 7(c) and stator current characteristics 7(d) are shown in fig.7 under steady state operation.

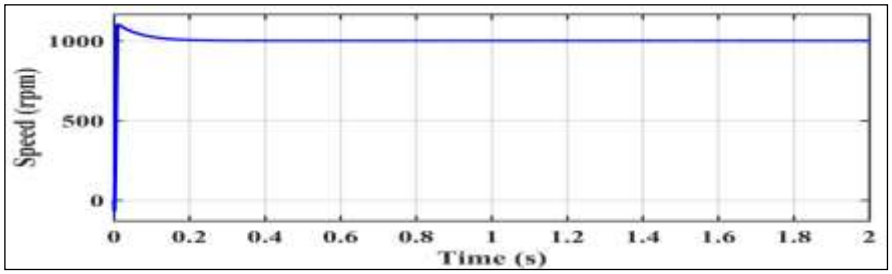

Figure 7(a): Speed(rpm) v/s Time(s).

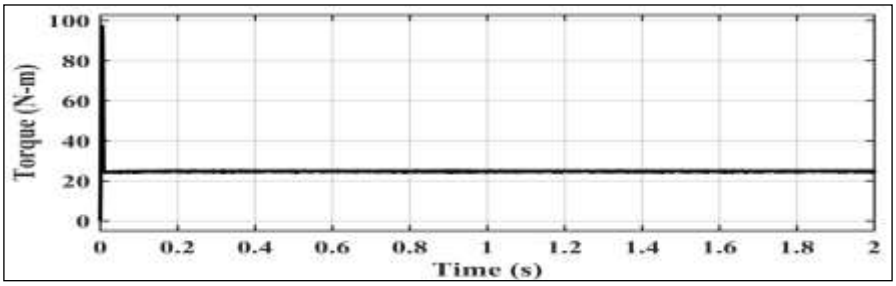

Figure 7(b): Torque(N-m) v/s Time(s).

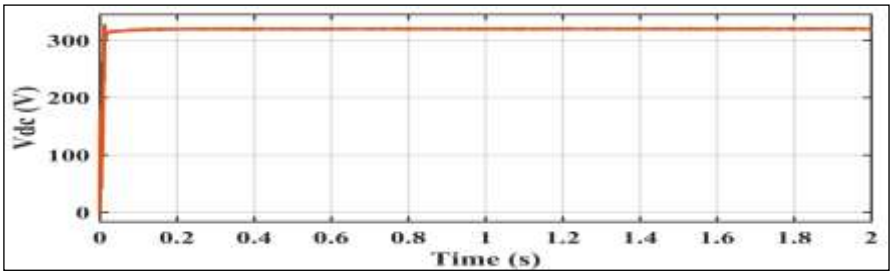

Figure 7(c): V_{dc} (v) v/s Time (s).

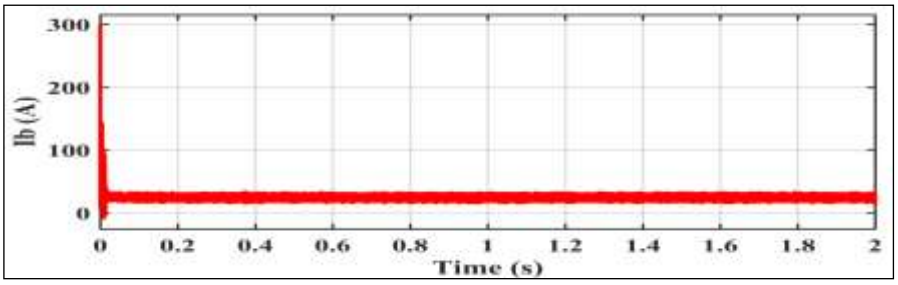

Figure 7(d): Ib (A) v/s Time (s).

Figure 7: Simulation results of the PMSM drive under steady-state operation.
Source: Authors, (2026).

Fig.7 shows that the Simulation test results of the PMSM drive under steady-state operation. Fig7(a), it is observed that PMSM with EV drive system initially the speed raises above the rated speed because of the rapid acceleration of torque and then the 0.2s speed is stabilizes and it reaches the rated speed of 1000 rpm proportionately maintain constant, validating its effectiveness for EV DC-bus capacitor discharge. Fig7(b) shows torque response reached peak value approximately 95Nm without damping oscillations because of the controller applies maximum acceleration torque to reach the reference speed rapidly, After the motor reaches the constant speed, therefore, the electromagnetic torque decreases and confirming stable performance of torque 25Nm during DC-bus discharge in EV. Fig 7(c) shows DC-bus voltage reached 340V because of the DC-bus capacitor draws a large inrush current.

After charging, the control system regulates the bus voltage, causing it to reduce and stabilize at the rated level and then maintained constant 320V, indicating stable regulation during capacitor discharge in EV. Fig 7(d) shows that the stator current initialy reached 300A peak value because of the motor needs a big initial torque to start moving, so the controller sends a large current for a short time and the fraction of seconds will falldown to low steady value and maintaining constant for confirming safe and controlled discharge in the EV PMSM drive. and then decreased 50A with high settling time and maintained constantly without any damping oscillations.

Case:II The dynamic behavior of the PMSM drive system: ANFIS for EV

The PMSM drive system under ANFIS control simulation model is tested with multiple speed transitions under a constant load that is 25Nm. The motor operated at different speeds 1000 rpm, 500 rpm, 300 rpm, 600 rpm, 800 rpm and 1000rpm. Throughout these variations, the ANFIS controller ensured fast speed tracking with negligible steady-state error and minimal overshoot. The dq-axis currents adapted smoothly, maintaining flux and torque control, while the electromagnetic torque showed minimal ripple. The dc-bus voltage (320V), battery voltage (130V), and current (25A,) remained stable, confirming effective power management.

The ANFIS-controlled PMSM drive demonstrated excellent dynamic performance and stability, making it well-suited for electric vehicle. The corresponding test output results speed characteristics 8(a), torque characteristics 8(b), DC bus voltage 8(c) and stator current characteristics 8(d) are shown in fig.8 under dynamic state operation.

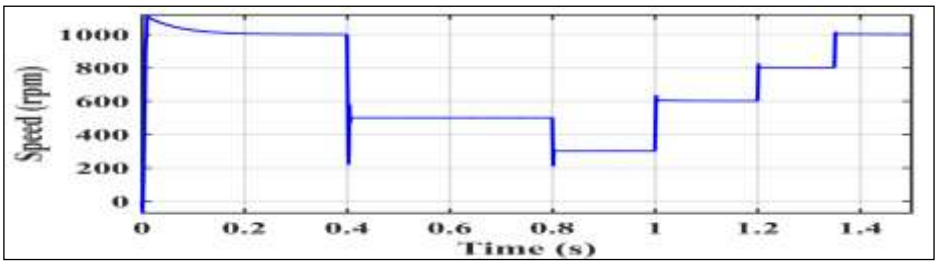

Figure 8(a): Speed(rpm) v/s Time(s).

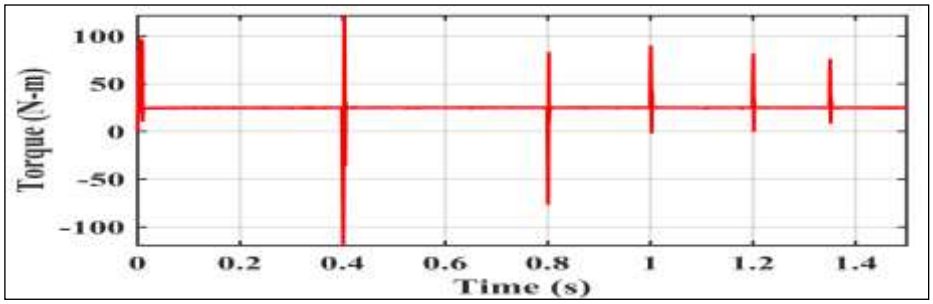

Figure 8(b): Torque (N-m) v/s Time(s).

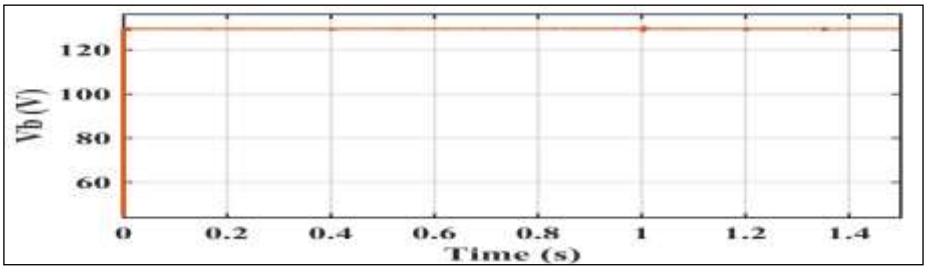

Figure 8(c): Vb (v) v/s Time(s).

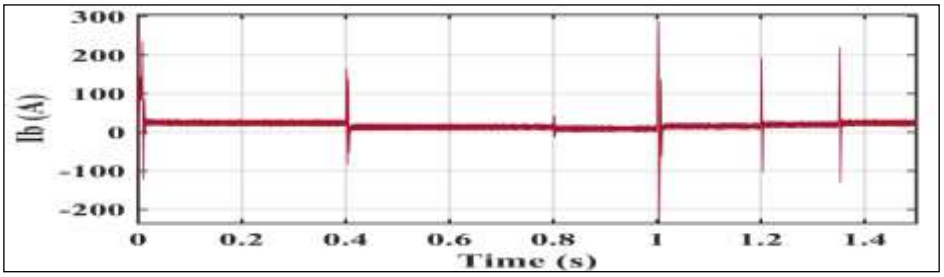

Figure 8(d): Ib(A) v/s Time(s).

Figure.8: Simulation Results under Dynamic Behavior of the PMSM Drive System.
Source: Authors, (2026).

Figure 8 shows that the Simulation test results of the PMSM drive under dynamic state operation. From the fig.8(a) observed that initially the speed shows peak value in a fraction of seconds and slightly settles the rated speed 1000 rpm because of the rapid acceleration of torque and it continuous and slowly step down to 500rpm at 0.4 s, after that it will continues and step down to 300rpm at 0.8s proportionately with 0.2 s time intervals the speed can be reaches to 1000rpm at 1.6s this process is analyzing until to reach the steady state. The motor tracks each reference level accurately, confirming strong dynamic response in EV drive conditions. Multiple speeds are used to evaluate controller performance under varying operating points.Fig. 8(b) shows torque variations in both positive and negative directions at different time intervals like 0.1s the load torque is 95Nm and then decreases to the statutory load limit 25Nm maintained with constant without damping oscillations at 0.4s, 0.8s and 1.4s respectively it indicating smooth transitions between motoring and regenerative modes with fast and controlled response.

Figure 8(c) shows that the DC-bus voltage stays around 125 V, confirming stable regulation during EV capacitor discharge. Fig 8(d) shows the range of current 20 A during normal operation. The speed reference changes, a sharp transient current spike at 0.4 s raised to nearly +180 A and then drops to –150 A as the motor responds to the speed reduction. The transient peaks at 0.8 s, 1.0 s, 1.2 s, and 1.4 s, where the current briefly reached values between 150-200 A, after each transient, the current quickly returns to its steady value around 10-20 A discharge current stays close to zero with different intervals only brief switching transients, demonstrating effective current regulation and stable capacitor discharge in the EV PMSM drive.

VI. ESO CONTROLLER FOR WINDING BASED SAFE DISCHARGE OF DC-BUS CAPACITOR

The simulation model of ESO controller as shown in fig.9. The Extended State Observer (ESO) controller is evaluated for the proposed winding-based safe discharge method in PMSM drives. During emergencies, the stator windings dissipate the dc-bus capacitor's stored energy after an initial flux-enfeebling d-axis current triggers rapid voltage reduction. The ESO accurately estimated and compensated for disturbances such as copper and switching losses, ensuring smooth, stable voltage decay without rebound. The simulation test results of the system as shown in fig 10(a) speed characteristics, fig 10(b) bus voltage characteristics, fig 10(c) torque respectively.

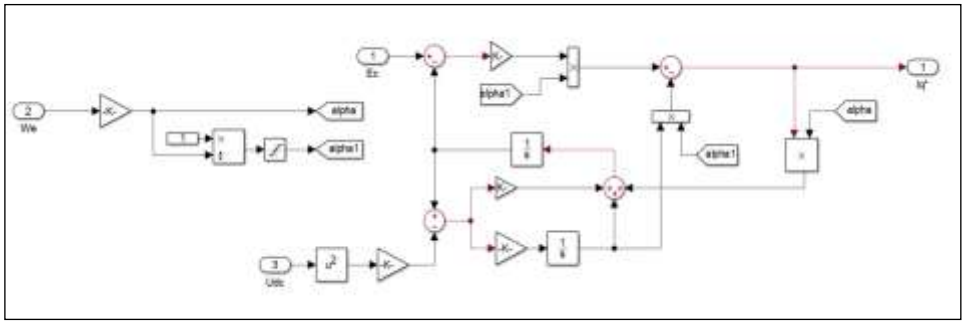

Figure 9: Simulation mode of ESO controller.
Source: Authors, (2026).

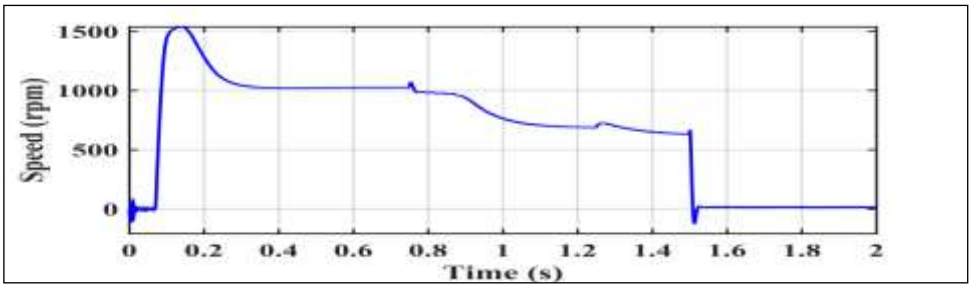

Figure 10(a): Speed(rpm) v/s Time(s).

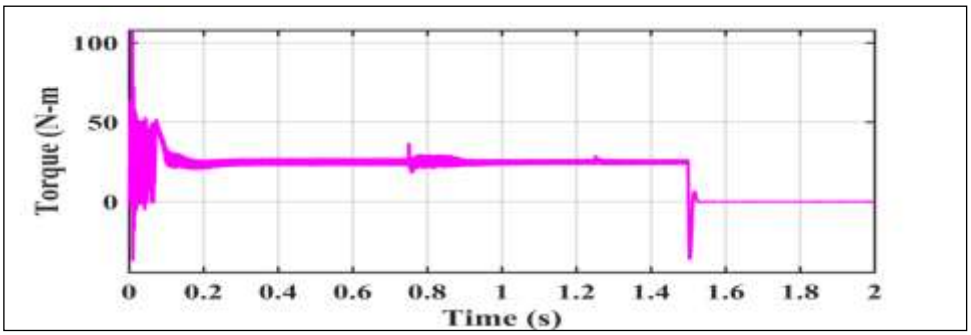

Figure 10(b) : Torque (N-m) v/s Time(s).

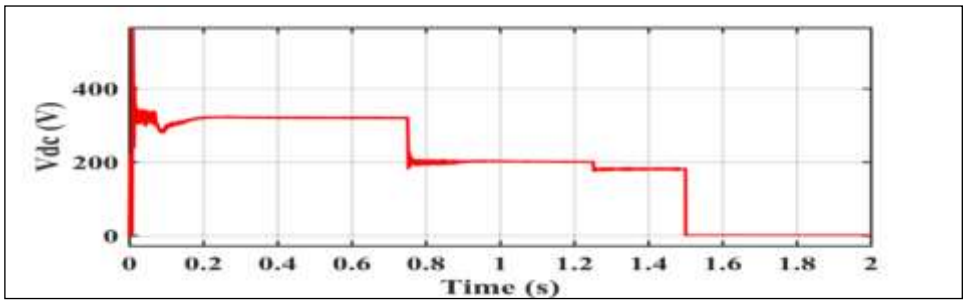

Figure 10(c): Vdc(v) v/s Time(s).

Figure 10: Simulation Results of ESO-Based Winding DC-Bus Capacitor for Safe Discharge.
Source: Authors, (2026).

From the simulation test results it is observed that fast discharge to safe voltage levels within limits compared to conventional methods, the ESO based approach achieved faster response, better disturbances rejection, and higher robustness confirming its effectiveness for safe PMSM operation in EV fault conditions. Fig.10 shows that the Simulation test results of the ESO controller for winding based safe discharge of dc bus capacitor. From the fig10(a) it is observed that PMSM speed during discharge the speed raises high peak around 1500 rpm due to the fast corrective action of the ESO, stabilizes near 1000 rpm, then gradually decreases in steps until it reaches zero, indicating controlled deceleration.

Figure 10(b) it is observed that the torque initially raised 100 Nm due to the startup transient and then settles around 40-45 Nm. A small disturbance appears near 0.8 s, 1.45 s the torque drops sharply to nearly 0 Nm, after it remains constant. Fig10(c) it is observed that the DC-bus voltage raised 390 V due to the initial transient, then stabilizes 300 V. At 0.8 s and 1.2 s it drops in steps to around 200 V and 170 V, and finally falls to 20 V at 1.4 s, indicating full capacitor discharge. Finally from the simulation test results are summarized compared to conventional methods with that of the proposed method which is tabulated in table.3.

Table:3 Comparison of test results.

Performance Criteria	PI Controller	Fuzzy Controller	ANN Controller	ANFIS Controller
Steady-State Speed (1000 rpm)	Acceptable regulation but small steady-state error present	Improved error reduction vs PI; dependent on rule accuracy	Good accuracy with reduced ripple but training-dependent	**Negligible error; precise tracking of 1000 rpm**
Dynamic Speed Transitions(1000 → 500 → 300 → 600 → 800 → 1000 rpm at 25 Nm load)	Slow response with overshoot and long settling	Faster than PI but moderate oscillations	Fast response; oscillations still exist	**Fastest response; minimal overshoot; shortest settling time**
Torque Ripple (25Nm)	High ripple	Moderate reduction depending on rules	Reduced ripple but still noticeable	**Smooth torque; minimal ripple**
dq-Axis Current Stability(25A)	Moderate stability	Good stability	Sensitive to parameter/training mismatch	**Excellent stability**
DC-Bus Voltage Regulation (320 V)	Poor stability during variations	Moderate performance	Good but with small fluctuations	**Stable and well-regulated at 320V**
Battery Operating Stability(130 V, 25 A)	Stable but slower dynamics	Good adaptation	Some fluctuations under disturbances	**Stable with strong disturbance rejection**

Source: Authors, (2026).

From the table.3 it is observed that the overall performance of the proposed control strategy for PMSM with EV system.

PI Controller: Shows acceptable steady-state response but suffers from slow transients and higher torque ripple. Stability reduces when dc-bus voltage drops during discharge.

Fuzzy Controller: Improves speed tracking and reduces ripple compared to PI. However, performance depends strongly on rule tuning and operating conditions.

ANN Controller: Provides faster dynamic response and better current regulation. Stability is affected by parameter variations outside the trained region, causing small fluctuations during discharge events.

ANFIS Controller: Delivers the best overall performance with fast settling, negligible speed error, smooth torque, and stable dq-axis currents maintains strong robustness against dc-bus capacitor discharge disturbances in EV operation.

VII CONCLUSIONS

The proposed control strategy discharge mechanism operates through two distinct stages to ensure rapid and controlled voltage reduction effectively addressed the limitations with active discharge circuits. The Simulation results confirmed that the two-stage discharge process, consisting of rapid flux-enfeebling current injection followed by ESO regulated voltage control, ensured a fast reduction of the dc-bus voltage to safe levels while preventing current and voltage overshoot. However the winding-based safe discharge method for the dc-bus capacitor in PMSM-driven electric vehicles, supported by ESO-based regulation and ANFIS-based speed control of electric vehicle.

The ESO demonstrated strong capability in estimating and compensating disturbances. However the integration of ESO based capacitor discharge with ANFIS based speed regulation provides a comprehensive solution that enhances both safety during emergencies and performance during normal driving operations. The proposed method shows strong potential for practical deployment in electric vehicle drive systems, ensuring passenger safety, reliable operation, and improved energy efficiency. Finally the proposed methodology ensures that safe voltage discharge during fault scenarios and enhanced the performance during standard operation, offering a reliable, intelligent and cost efficient solution for modern electric vehicle drive system.

VIII. AUTHOR'S CONTRIBUTION

Conceptualization: Chevuru Mahima, Ch. Chengaiah.
Methodology: Chevuru Mahima, Ch. Chengaiah.
Investigation: Chevuru Mahima, Ch. Chengaiah.
Discussion of results: Chevuru Mahima, Ch. Chengaiah.
Writing – Original Draft: Chevuru Mahima, Ch. Chengaiah.
Writing – Review and Editing: Chevuru Mahima, Ch. Chengaiah.
Resources: Chevuru Mahima, Ch. Chengaiah.
Supervision: Chevuru Mahima, Ch. Chengaiah.
Approval of the final text: Chevuru Mahima, Ch. Chengaiah.

IX.REFERENCES

[1] S. Sakunthala, R. Kiranmayi and P. N. Mandadi, "A Review on Speed Control of Permanent Magnet Synchronous Motor Drive Using Different Control Techniques," 2018 International Conference on Power, Energy, Control and Transmission Systems (ICPECTS), Chennai, 2018, pp. 97-102, doi: 10.1109/ICPECTS.2018.8521574.

[2] V. M. Bida, D. V. Samokhyalov and F. S. Al-Mahturi, "PMSM vector control techniques – A survey," 2018 IEEE Conference of Russian Young Researchers in Electrical and Electronic Engineering (EIConRus), Moscow, 2018, pp. 577-581, doi: 10.1109/EIConRus.2018.8317164

[3] Y. Kung, Risfendra, Y. Lin and L. Huang, "FPGA-based sensorless controller for PMSM drives using sliding mode observer and phase locked loop," 2016 International Conference on Applied System Innovation (ICASI), Okinawa, 2016, pp. 1-4, doi:10.1109/ICASI.2016.7539798.

[4] S. Chen and H. Hoai, "Studying an Adaptive Fuzzy PID Controller for PMSM with FOC based on MATLAB Embedded Coder," 2019 IEEE International Conference on Consumer Electronics - Taiwan (ICCE-TW), YILAN, Taiwan, 2019, pp. 1-2, doi: 10.1109/ICCE TW46550.2019.8991743.

[5] M. B. B. Sharifian, T. Herizchi and K. G. Firouzjah, "Field oriented control of permanent magnet synchronous motor using predictive space vector modulation," 2009 IEEE Symposium on Industrial Electronics & Applications, Kuala Lumpur, 2009, pp. 574-579, doi: 10.1109/ISIEA.2009.5356385.

[6] [Online] https://in.element14.com/motor-control-permanent-magnet-sync-motor-pmsm- technology

[7] F. Korkmaz, İ. Topaloğlu, M. F. Çakir and R. Gürbüz, "Comparative performance evaluation of FOC and DTC controlled PMSM drives," 4th International Conference on Power Engineering, Energy and Electrical Drives, Istanbul, 2013, pp. 705-708, doi: 10.1109/PowerEng.2013.6635696.

[8] P. Sala-Perez, S. Galceran-Arellano and D. Montesinos-Miracle, "A sensorless stable V/f control method for a five-phase PMSM," 2013 15th European Conference on Power Electronics and Applications (EPE), Lille, 2013, pp. 1-10, doi: 10.1109/EPE.2013.6631943.

[9] K. Yang, X. Yang, H. Xie, Y. Liu, Y. Zhang and X. Wei, "Stable sensorless V/f and cosφ =1 control for permanent magnet synchronous motor drives," 2014 17th International Conference on Electrical Machines and Systems (ICEMS), Hangzhou, 2014, pp. 3564-3568, doi: 10.1109/ICEMS.2014.7014107.

[10] G. Xie, K. Lu, S. K. Dwivedi, J. R. Rosholm and F. Blaabjerg, "Minimum-Voltage Vector Injection Method for Sensorless Control of PMSM for Low-Speed Operations," in IEEE Transactions on Power Electronics, vol. 31, no. 2, pp. 1785-1794, Feb. 2016, doi: 10.1109/TPEL.2015.2426200.

[11] M. Konghirun and L. Xu, "A Fast Transient-Current Control Strategy in Sensorless Vector Controlled Permanent Magnet Synchronous Motor," in IEEE Transactions on Power Electronics, vol. 21, no. 5, pp. 1508-1512, Sept. 2006, doi: 10.1109/TPEL.2006.882419.

[12] S. Li, H. Won, X. Fu, M. Fairbank, D. C. Wunsch and E. Alonso, "Neural-Network Vector Controller for Permanent-Magnet Synchronous Motor Drives: Simulated and Hardware-Validated Results," in IEEE Transactions on Cybernetics, vol. 50, no. 7, pp. 3218-3230, July 2020, doi: 10.1109/TCYB.2019.2897653.
[13] S. Fartash Toloue, S. H. Kamali and M. Moallem, "Multivariable sliding-mode extremum seeking PI tuning for current control of a PMSM," in IET Electric Power Applications, vol. 14, no. 3, pp. 348-356, 3 2020, doi: 10.1049/iet-epa.2019.0033.

[14] In-Cheol Baik, Kyeong-Hwa Kim and Myung-Joong Youn, "Robust nonlinear speed control of PM synchronous motor using boundary layer integral sliding mode control technique," in IEEE Transactions on Control Systems Technology, vol. 8, no. 1, pp. 47-54, Jan. 2000, doi: 10.1109/87.817691. 89

[15] D. Liang, J. Li, R. Qu and W. Kong, "Adaptive Second-Order Sliding-Mode Observer for PMSM Sensorless Control Considering VSI Nonlinearity," in IEEE Transactions on Power Electronics, vol. 33, no. 10, pp. 8994-9004, Oct. 2018, doi: 10.1109/TPEL.2017.2783920.

[16] Mohamed, Y.A.I. Design and Implementation of a Robust Current-Control Scheme for a PMSM Vector Drive With a Simple Adaptive Disturbance Observer. IEEE Transactions on Industrial Electronics 2007, 54, 1981–1988.

[17] T. Türker, U. Buyukkeles and A. F. Bakan, "A Robust Predictive Current Controller for PMSM Drives," in IEEE Transactions on Industrial Electronics, vol. 63, no. 6, pp. 3906-3914, June 2016, doi: 10.1109/TIE.2016.2521338.

[18] S. Carpiuc and C. Lazar, "Fast Real-Time Constrained Predictive Current Control in Permanent Magnet Synchronous Machine-Based Automotive Traction Drives," in IEEE Transactions on Transportation Electrification, vol. 1, no. 4, pp. 326-335, Dec. 2015, doi: 10.1109/TTE.2015.2482223.
[19] W. Wang, Y. Fan, S. Chen and Q. Zhang, "Finite control set model predictive current control of a five-phase PMSM with virtual voltage vectors and adaptive control set," in CES Transactions on Electrical Machines and Systems, vol. 2, no. 1, pp. 136-141, March 2018, doi: 10.23919/TEMS.2018.8326460.

[20] G. Prior and M. Krstic, "Quantized-Input Control Lyapunov Approach for Permanent Magnet Synchronous Motor Drives," in IEEE Transactions on Control Systems Technology, vol. 21, no. 5, pp.

[21] C. Gong, Y. Hu, C. Gan, G. Chen and M. Alkahtani, "Modeling, Analysis, and Attenuation of Uncontrolled Generation for IPMSM Based Electric Vehicles in Emergency," in IEEE Trans. Ind. Electron., vol. 67, no. 6, pp. 4453-4462, June 2020.

[22] J. Liu, C. Gong, Z. Han and H. Yu, "IPMSM Model Predictive Control in Flux-Weakening Operation Using an Improved Algorithm," in IEEE Trans. Ind. Electron., vol. 65, no. 12, pp. 9378 9387, Dec. 2018.

[23] Y. Zhang, J. Jin and L. Huang, "Model-Free Predictive Current Control of PMSM Drives Based on Extended State Observer Using Ultralocal Model," in IEEE Trans. Ind. Electron., vol. 68, no. 2, pp. 993-1003, Feb. 2021.

[24] M. Fliess and C. Join, "Model-free control," Int. J. Control, vol. 86, no. 12, pp. 2228–2252, 2013. [25] C. Lin, T. Liu, J. Yu, L. Fu and C. Hsiao, "Model-Free Predictive Current Control for Interior Permanent-Magnet Synchronous Motor Drives Based on Current Difference Detection Technique," in IEEE Trans. Ind. Electron., vol. 61, no. 2, pp. 667-681, Feb. 2014.

[25] C. Lin, T. Liu, J. Yu, L. Fu and C. Hsiao, "Model-Free Predictive Current Control for Interior Permanent-Magnet Synchronous Motor Drives Based on Current Difference Detection Technique," in IEEE Trans. Ind. Electron., vol. 61, no. 2, pp. 667-681, Feb. 2014.

[26] S. Zhou, J. Liu, L. Zhou and Y. Zhang, DQ Current Control of Voltage Source Converters with a Decoupling Method Based on Preprocessed Reference Current Feed-forward, in IEEE Trans. Power Electron., vol. 32, no. 11, pp. 8904-8921, Nov. 2017.

[27] X. Zhang and J. Yang, "A Robust Flywheel Energy Storage System Discharge Strategy for Wide Speed Range Operation," in IEEE Trans. Ind. Electron., vol. 64, no. 10, pp. 7862-7873, Oct. 2017.